

MAPPING THE GALACTIC CENTER WITH GRAVITATIONAL WAVE MEASUREMENTS USING PULSAR TIMING

BENCE KOCSIS,¹ ALAK RAY,^{2,3} SIMON PORTEGIES ZWART⁴

¹Harvard-Smithsonian Center for Astrophysics, 60 Garden Street, Cambridge, MA 02138, bkocsis@cfa.harvard.edu

²Harvard-Smithsonian Center for Astrophysics, 60 Garden Street, Cambridge, MA 02138 and ³Tata Institute of Fundamental Research, Homi Bhabha Road, Mumbai 400005, India, akr@tifr.res.in and

⁴Leiden Observatory, Leiden University, P.O. Box 9513, 2300 RA Leiden, The Netherlands, spz@strw.leidenuniv.nl

Draft version October 21, 2018

ABSTRACT

We examine the nHz gravitational wave (GW) foreground of stars and black holes (BHs) orbiting SgrA* in the Galactic Center. A cusp of stars and BHs generates a continuous GW spectrum below 40 nHz; individual BHs within 1 mpc to SgrA* stick out in the spectrum at higher GW frequencies. The GWs and gravitational near-field effects can be resolved by timing pulsars within a few pc of this region. Observations with the Square Kilometer Array (SKA) may be especially sensitive to intermediate mass black holes (IMBHs) in this region, if present. A 100 ns–10 μ s timing accuracy is sufficient to detect BHs of mass 1000 M_{\odot} with pulsars at distance 0.1–1 pc in a 3 yr observation baseline. Unlike electromagnetic imaging techniques, the prospects for resolving individual objects through GW measurements improve closer to SgrA*, even if the number density of objects increases inwards steeply. Scattering by the interstellar medium will pose the biggest challenge for such observations.

Subject headings: galaxies: nuclei – gravitational waves – pulsars

1. INTRODUCTION

There is a great ongoing effort to use pulsar timing arrays to detect gravitational waves (GWs) in the nHz frequency bands. GWs, if present, modify the exceptionally regular arrival times of pulses from radio pulsars. Observations of a correlated modulation in the time of arrivals (TOAs) of pulses from a network of highly stable millisecond pulsars (MSPs) across the sky can be used to detect GWs (Detweiler 1979; van Haasteren et al. 2011). Existing pulsar timing arrays (PTAs) utilize the brightest and most stable nearby MSPs in the Galaxy.

At nHz frequencies, the GW background is expected to be dominated by cosmological supermassive black hole (SMBH) binaries (Rajagopal & Romani 1995; Jaffe & Backer 2003; Wyithe & Loeb 2003; Sesana et al. 2004). Only a few studies considered the GW signal from nearby sources. Lommen & Backer (2001) showed that pulsar signals would be sensitive to a putative SMBH binary in the Galactic Center with mass ratio 0.06, however, such a binary would have other dynamical consequences which are not observed (Yu & Tremaine 2003). Further, Jenet et al. (2004) showed that the nearby extragalactic source 3C 66B does not contain a massive SMBH binary, because PTAs do not observe the expected GW modulation. Blandford et al. (1987) and de Paolis et al. (1996) examined if the variable gravitational field of nearby stars could be detected using pulsar timing in the cores of globular clusters, and similarly, Jenet et al. (2005) considered the possibility of detecting GWs from intermediate mass black hole binary sources using pulsars in the cluster.

In this paper, we examine the prospects for directly detecting the GW foreground and gravitational near-field effects of the Galactic Center (GC) using pulsars in the vicinity of this region (see also Ray & Kluzniak 1994). We estimate the foreground (in contrast with the cosmological background of GWs) generated by the dense population of stars and compact objects (COs) in the GC, including about 20,000 stellar mass black holes (BHs) (Morris 1993; Freitag et al. 2006a)

and perhaps a few intermediate mass black holes (IMBHs) of mass $10^3 M_{\odot}$ (Portegies Zwart et al. 2006). As these objects are much more massive than regular stars populating the GC, they segregate and settle to the core of the central star cluster. The emitted GW signal falls in the nHz range, well in the PTA frequency band. While this foreground signal may be faint at kpc distances in the Galaxy as Jenet et al. (2004) discussed, it may exceed the GW background locally, near the GC. The present generation of PTAs, achieve an upper limit of the characteristic stochastic GW background amplitude of the order $h_c \lesssim 6 \times 10^{-15}$ at $f \sim 1/\text{yr} \sim 30 \text{ nHz}$ (van Haasteren et al. 2011), while the theoretical prediction is $h_c \sim 9 \times 10^{-16} (f \text{ yr})^{-2/3}$ (Kocsis & Sesana 2011, and see § 4.1 below). We estimate the level of pulsar timing accuracy necessary (i) to constrain the mass of IMBHs in the GC using pulsars in the GC neighborhood to a level better than existing constraints, or (ii) to resolve the central cusp of stellar mass objects.

While a large population of pulsars is expected to reside in the Galactic Center (Pfahl & Loeb 2004), their detection is quite challenging. It requires high sensitivity ($\gtrsim 0.01 \mu\text{Jy}$) at relatively high radio frequencies ($\gtrsim 10 \text{ GHz}$) where the pulse smearing due to the scattering of the ISM is less severe (Lazio & Cordes 1998). Since pulsars have a steep radio frequency spectrum, $S_{\nu} \propto \nu^{-1.6}$ to $\nu^{-1.8}$ (Kramer et al. 1998), the high frequency of observation makes them very faint and thus difficult to detect and time. Note however, that Keith et al. (2011) have successfully detected nine radio pulsars at a frequency of 17 GHz, including the detection of a millisecond pulsar and a magnetar with an indication that the spectral index may flatten above 10 GHz. The future Square Kilometer Array is expected to find several thousand regular pulsars, and a few MSPs in the GC (Cordes et al. 2004; Cordes 2007; Smits et al. 2009; Macquart et al. 2010; Smits et al. 2011). High time resolution surveys recently found 5 millisecond pulsars in mid galactic latitudes (Bates et al. 2011), 3 within 100 pc of the Galactic Center (Johnston et al. 2006; Deneva et al. 2009). Based on the properties of nearby pulsars

and nondetections in a targeted observation, Macquart et al. (2010) recently put an upper limit of 90 regular pulsars within the central 1 pc. It is likely that the timing accuracy of these pulsars in the GC will be much worse than those in the local Galactic neighborhood. However, the GW signal may be much stronger near the GCs to make a GW detection possible with a lower timing accuracy.

We adopt geometrical units $G = c = 1$, and suppress the G/c^2 and G/c^3 factors to change mass to length or time units.

2. BLACK HOLES IN THE GALACTIC CENTER

2.1. Stellar mass BHs

The number density of objects in a relaxed galactic cusp orbiting around an SMBH with semimajor axis a is

$$n_*(a) = \frac{3-\alpha}{4\pi} N_* \left(\frac{a}{\text{pc}} \right)^{-\alpha} \text{pc}^{-3}, \quad (1)$$

where N_* is the total number of objects within 1 pc, and $\alpha = 7/4$ for a stationary Bahcall-Wolf cusp (Bahcall & Wolf 1976; Binney & Tremaine 2008). If the mass function in the cusp is dominated by heavy objects, the density of light and heavy objects relaxes to a profile with $\alpha \sim 3/2$ and $\alpha \sim 7/4$, while in the opposite case as steep as $\sim 9/4$ to 3 for the heavy objects (Alexander & Hopman 2009; Keshet et al. 2009). These stationary profiles have a constant inward flux of objects which are eventually swallowed by the SMBH and replenished from the outside. We take the theoretically expected value $N_* = 20,000$ for stellar mass black holes of mass $m_* = 10M_\odot$ within 1 pc (Morris 1993; Miralda-Escudé & Gould 2000; Freitag et al. 2006a) and assume $\alpha_{*,\text{BH}} = 2$.

The eccentricity distribution for a relaxed thermal distribution of an isotropic cusp is such that the number of objects in a de bin is proportional to $dN \propto e de$, independent of semimajor axis (Binney & Tremaine 2008).

2.2. Intermediate mass BHs

Intermediate mass black holes (IMBHs) are expected to be created by the collapse of Pop III stars in the early universe (Madau & Rees 2001), runaway collisions of stars in the cores of globular clusters (Portegies Zwart & McMillan 2002; Freitag et al. 2006b), or the mergers of stellar mass black holes (O’Leary et al. 2006). If globular clusters sink to the galactic nucleus due to dynamical friction, they are tidally stripped and deposit their IMBHs in the Galactic nucleus. Then the IMBHs settle to the inner region of the nucleus by mass segregation with stars. Portegies Zwart et al. (2006) predict that the inner 10 pc of the GC hosts 50 IMBHs of mass $M \sim 10^3 M_\odot$.

There are very few unambiguous observations of intermediate mass black holes (IMBHs) in the Universe (Miller & Colbert 2004). Ultraluminous X-ray sources provide the best observational candidates. In particular, HLX-1 in ESO 243-49 is found to have a mass between $3 \times 10^3 M_\odot \lesssim M \lesssim 3 \times 10^5 M_\odot$ (Davis et al. 2011). In the Galactic Center, 0.13 pc projected distance from SgrA*, IRS 13E is a dense concentration of massive stars, which has been argued to host an IMBH of mass between 10^3 and $10^4 M_\odot$ (Maillard et al. 2004), however the observed acceleration constraints make an IMBH interpretation in IRS 13E presently unconvincing (Fritz et al. 2010). Astrometric observations of the radio source SgrA* corresponding to the SMBH can be used to place an upper limit of the mass of an IMBH to $M \lesssim 10^4 M_\odot$

in 5–500 mpc (Reid & Brunthaler 2004). Further, an IMBH could have served to deliver the observed young stars in the GC (Hansen & Milosavljević 2003; Fujii et al. 2009), eject hypervelocity stars (Yu & Tremaine 2003; Gualandris et al. 2005), create a low-density core in the GC (Baumgardt et al. 2006), efficiently randomize the eccentricity and orientations of the observed S-star orbits (Merritt et al. 2009), and may have contributed to the SMBH growth (Portegies Zwart et al. 2006). These dynamical arguments can be used to place independent limits on the existence and mass of IMBHs in the Galactic Center (see Genzel et al. 2010, for a review). Future observation of the pericenter passage of the shortest period known star S2 may improve this limit to a few $\times 10^3 M_\odot$ in 2018 (Gualandris et al. 2010), and even better limits will be possible by imaging SgrA* with Event Horizon Telescope (EHT), a millimeter/submillimeter very long baseline interferometer (VLBI) (Broderick et al. 2011). We examine whether pulsar timing could detect an IMBH with parameters not excluded by existing observations, or be used to place independent limits.

2.3. Loss cone

A depleted region is formed in phase space if objects are removed at a rate faster than they are replenished from outside by inward diffusion. In this region, Eq. (1) is no longer valid. The dominant source of removing stars is tidal disruption or physical collisions, while for BHs it is GW capture by the SMBH.

The objects with initial conditions (a, e) fall in and merge with the SMBH due to GW emission in a time

$$t_{\text{mg}} = \frac{5\kappa}{256} \frac{a^4}{m_* M_\bullet^2} (1-e^2)^{7/2} = 36 \kappa m_3^{-1} a_{\text{mpc}}^4 (1-e^2)^{7/2} \text{Gyr}. \quad (2)$$

where $a_{\text{mpc}} = a/\text{mpc}$, $m_3 = m_*/10^3 M_\odot$, and $1 \leq \kappa < 1.8$ is a weakly dependent function of eccentricity (Peters 1964). Assuming $e \gg 0$ and $t_d \leq t_{\text{mg}}$, the minimum semimajor axis is

$$a_{\text{lc}} = 0.4 \text{ mpc} \times m_3^{1/4} (1-e)^{-7/8} t_{d,9}^{1/4}, \quad (3)$$

where the inward diffusion time is parameterized as $t_{d,9} = t_d/10^9 \text{ yr}$, and we assumed $f \sim f_p \sim (1-e)^{-3/2} f_{\text{orb}}$ (see Eq. (A5)). For stellar mass BHs, the inward diffusion time is related to two-body relaxation (Binney & Tremaine 2008). Depending on the number and masses of BHs, O’Leary et al. (2009) find that $0.1 \lesssim t_{d,9} \lesssim 10$. For IMBHs, the inward diffusion is due to dynamical friction and the scattering of stars. This process is initially faster than the relaxation timescale, but then slows down ($t_{d,9} \sim 10$) as stars on crossing orbits are ejected by the IMBH (Gualandris & Merritt 2009). The number density inside a_{lc} is expected to be much less than that of Eq. (1). In such a state, the eccentricity of an IMBH is increased (Matsubayashi et al. 2007; Sesana 2010; Iwasawa et al. 2011). However, a possible triaxiality of the cluster might result in the refilling of the loss-cone and shorter inward migration timescales (Khan et al. 2011; Preto et al. 2011; Gualandris & Merritt 2012).

3. GRAVITATIONAL WAVES FROM THE GALACTIC CENTER

We start by reviewing the essential formulas to derive the GWs generated by a population of binaries with circular orbits, then turn to the general eccentric case. We discuss other details of the spectrum, regarding the high frequency cutoff and splitting into discrete peaks, at the end of the section.

3.1. Unresolved circular sources

The GW frequency for a circular orbit is twice the orbital frequency, $f = 2f_{\text{orb}}$, and the corresponding orbital radius is

$$r(f) = M_{\bullet} (\pi M_{\bullet} f)^{-2/3} = 2.6 f_8^{-2/3} \text{ mpc}. \quad (4)$$

where $f_8 = f/(10^{-8} \text{ Hz})$. In the last equality, the mass of the central SMBH in SgrA* is taken as $M_{\bullet} = 4.3 \times 10^6 M_{\odot}$ (Gillessen et al. 2009). To put in context, 20 mpc (i.e. about 4,100 AU) is the distance to the observed S-stars, the innermost star, S2, has semimajor axis 4 mpc and pericenter 0.8 mpc, and the stellar disk of massive young stars extends down to 30 mpc (Genzel et al. 2010).

The RMS strain generated by an object of mass m_* orbiting around a SMBH of mass M_{\bullet} on a circular orbit at distance D from the source in one GW cycle is

$$h_0(f) = \sqrt{\frac{32}{5}} \frac{M_{\bullet} m_*}{D r(f)} = 8.8 \times 10^{-15} m_3 D_{\text{pc}}^{-1} f_8^{2/3}, \quad (5)$$

where $D_{\text{pc}} = D/\text{pc}$, $m_3 = m_*/(10^3 M_{\odot})$, and the 0 index will stand for zero eccentricity. The $\sqrt{32/5}$ prefactor accounts for RMS averaging the GW strain over orientation.

The GW strain of many independent sources with the same frequency but random phase adds quadratically. For a signal observed for time T , the spectral resolution is $\Delta f = 1/T$. Therefore the number of sources with overlapping frequencies is

$$\Delta N = \frac{dN}{dr} \left| \frac{dr}{df} \right| \frac{1}{T}. \quad (6)$$

The number of GW cycles observed in time T is fT . The integrated GW signal with frequency f is

$$h_c^2 = \Delta N (fT) h_0^2 = \frac{dN}{dr} \left| \frac{dr}{df} \right| f h_0^2 = \frac{dN}{d \ln f} h_0^2, \quad (7)$$

also called *characteristic spectral amplitude* (Phinney 2001). Therefore the characteristic GW amplitude from a population of sources can be interpreted as the RMS GW strain in a logarithmic frequency bin. Here dN/dr is the number of sources in a spherical shell and dr/df is to be evaluated using Eq. (4). Note that the final formula (7) is independent of T .¹

We can express h_c with the number density of objects using $dN/dr = 4\pi r^2 n_*(r)$, as

$$h_c^2(f) = \frac{8\pi}{3} r^3 n_*(r) h_0^2 = \frac{256\pi}{15} \frac{M_{\bullet} m_*^2}{D^2} (\pi M_{\bullet} f)^{-2/3} n_*[r(f)]. \quad (8)$$

Eq. (8) gives the root-mean-square (RMS) GW signal level drawing the stars or BHs from a density profile $n_*(r)$. The equation shows that the spectral shape is different from $f^{-2/3}$, describing the RMS cosmological background (Phinney 2001). Note that h_c is proportional to the RMS mass of objects which may exceed the mean for a multimass population. The GW signal for any one realization is well approximated by the RMS if $\Delta N \gg 1$. Close to the center (which corresponds to high f), ΔN is small, and the GW spectrum becomes spiky, which we discuss in § 3.3 below.

The GW foreground may be different from the above estimate for sources with significant eccentricity, for sources on

¹ This is true as long as the source distribution is effectively continuous in frequency space, so that individual sources are unresolved, but not for resolved discrete sources (see Eq. (13) and §. 3.3 below).

unbound orbits, or if they are non-periodic or evolve secularly during the observation, or if the population is anisotropic. We elaborate on the corresponding effects on the GWs in the subsections below, and discuss the characteristic GW frequency where the spectrum would be affected by the loss cone and small number statistics.

3.2. Eccentric periodic and burst sources

Here we summarize the modification of the above estimates due to eccentricity, and refer the reader to Appendix A for details.

For eccentric sources, the GW spectrum of individual sources is no longer peaked around $f = 2f_{\text{orb}}$. For mildly eccentric sources ($e \lesssim 0.3$), the GW spectrum is spiky, with discrete upper harmonics, $f = n f_{\text{orb}}$, with decreasing amplitude for $n > 2$. The observed width of each spectral peak is $\Delta f = 1/T$. For larger eccentricities, the upper harmonics are stronger than the $n = 2$ mode, and the peak frequency corresponds to the inverse pericenter passage timescale f_p , where 90% of the GW power is between $0.2 f_p < f < 3 f_p$.

The GWs are in the PTA frequency band if the pericenter passage timescale is less than the observation time, T . We distinguish two types of sources: *periodic* and *GW burst sources*.² Periodic sources have orbital periods shorter than T , or semimajor axis

$$a_{\text{per}} \leq 5.7 T_{10}^{2/3} \text{ mpc}. \quad (9)$$

At relatively low frequencies where small number and loss cone effects do not kick in, these sources generate a continuous GW spectrum which is similar to that given by the circular formula Eq. (13) within a factor 2, assuming an isotropic thermal eccentricity distribution (see Eq. (A12) and (A13) in Appendix A).

Sources with semimajor axes larger than Eq. (9) generate a GW burst during pericenter passage in the PTA band if their pericenter distance at close approach is less than Eq. (9). Only a small fraction of these burst sources contribute to the PTA measurements, the ones which are within time T from pericenter passage along their orbits during the observation. In Appendix A, we show that the stochastic background of burst sources is expected to be typically much weaker than the periodic sources, unless there are IMBHs on wide eccentric orbits.

3.3. Individually resolvable sources

The GW foreground generated by a population of objects is smooth if the average number per Δf frequency bin satisfies $\langle \Delta N \rangle \gg 1$. If the number density follows Eq. (1), and the total number within 1 pc is normalized as $\bar{N}_* = N_*/(2 \times 10^4)$, then the spectrum becomes spiky ($\langle \Delta N \rangle \leq 1$) above

$$f_{\text{res}} = 4.2 \times 10^{-8} \text{ Hz} \times 10^{9(\alpha-2)/(9-2\alpha)} \left[\frac{(3-\alpha)\bar{N}_*}{T_{10}} \right]^{3/(9-2\alpha)} \quad (10)$$

where $T_{10} = T/10 \text{ yr}$, and we used Eqs. (4) and (6) for circular orbits. The corresponding orbital radius is

$$r_{\text{res}} = 1.0 \text{ mpc} \times 10^{6(\alpha-2)/(2\alpha-9)} \left[\frac{T_{10}}{(3-\alpha)\bar{N}_*} \right]^{2/(9-2\alpha)} \quad (11)$$

² There are also ‘‘repeated burst’’ sources which are highly eccentric with orbital periods less than T , which satisfy Eq. (9) (Kocsis & Levin 2011). We do not distinguish repeated bursts from periodic sources here.

Sources within r_{res} generate distinct spectral peaks above frequency f_{res} . We refer to these sources as *resolvable*.

The total number of resolvable sources is

$$N_{\text{res}} = \int_0^{r_{\text{res}}} n_*(r) 4\pi r^2 dr = N_* \left(\frac{r_{\text{res}}}{\text{pc}} \right)^{3-\alpha} \quad (12)$$

$$= 20 \times 10^{9(\alpha-2)/(9-2\alpha)} \bar{N}_* \left(\frac{T_{10}}{(3-\alpha)\bar{N}_*} \right)^{2(3-\alpha)/(9-2\alpha)}.$$

Note that f_{res} , r_{res} , and N_{res} are exponentially sensitive to the density exponent: in a 10 year observation of $N_* = 20,000$ BHs, $f_{\text{res}} = (19, 42, 110)$ nHz, $r_{\text{res}} = (1.7, 1.0, 0.53)$ mpc, and $N_{\text{res}} = (7, 20, 70)$ for $\alpha = (1.75, 2, 2.25)$, respectively. Similarly, for $N_* = 50$ IMBHs, $f_{\text{res}} = (2.0, 3.8, 6.4)$ nHz, $r_{\text{res}} = (7.6, 5.1, 3.5)$ mpc, and $N_{\text{res}} = (1, 3, 12)$ for $\alpha = (2.25, 2.5, 2.75)$, respectively. If the supply of objects by two body relaxation is very slow, $t_d \gg 1$ Gyr, and the loss cone is empty (see § 2.3), then the number of resolvable sources can be much less. *The GW spectrum transitions from continuous to discrete inside the PTA frequency band, and the expected number of resolvable sources is typically non-negligible.*

For $f > f_{\text{res}}$, the GW spectrum is $h_c(f) = 0$, except for distinct frequency bins which include one resolvable source each. For the latter, the net GW signal amplitude in time T is

$$h_{c,1}(f) = (fT)^{1/2} h_0(f) = 1.6 \times 10^{-14} m_3 D_{\text{pc}}^{-1} T_{10}^{1/2} f_8^{7/6}. \quad (13)$$

Therefore $h_{c,1}(f)$ increases quickly for individual sources with decreasing orbital radius or increasing frequency. The prospects for detecting individual sources closer than r_{res} to SgrA* improves because the GW amplitude increases, while the confusion noise per frequency bin decreases (see Eq. (23) below for the corresponding timing residual).

Note that Eq. (13) corresponds to the GW polarization averaged integrated signal³ for stationary circular orbits. We derive $h_c(f)$ for eccentric periodic and burst sources in Appendix A. In that case, the GW power of each source is distributed over many harmonics, making the detection of individual sources potentially more challenging. However, GR pericenter precession leads to an overall amplitude modulation of the relative weights of the two GW polarizations (Königsdörffer & Gopakumar 2006). This effect increases inward, which may improve the prospects for separating individual sources.

3.4. Maximum GW frequency

What is the maximum GW frequency for objects outside of the loss-cone, for which the GW merger is still longer than the relaxation timescale? The maximal emitted GW frequency corresponding to Eq. (3) is

$$f_{\text{lc}} = 1.6 \times 10^{-7} \text{ Hz} \times m_3^{-3/8} (1-e)^{-3/16} t_{d,9}^{-3/8}, \quad (14)$$

where note that the dimensionless diffusion time is $0.1 \leq t_{d,9} \leq 10$ for multimass two-body relaxation models (see § 2.3), and we assumed $f \sim f_p \sim (1-e)^{-3/2} f_{\text{orb}}$ (see Eq. (A5)). The GW spectrum is expected to terminate above f_{lc} . Eq. (14) implies that $10 M_\odot$ BHs generate a GW background with a maximum frequency of around 10^{-6} Hz = (12 day)⁻¹ for mildly eccentric sources, and somewhat larger for more

³ More precisely, for circular sources, $h_c^2 = \langle \int_0^T (h_+^2 + h_\times^2) f dt \rangle$, where $\langle \cdot \rangle$ corresponds to averaging over source inclination. Note that throughout this manuscript $h_c(f)$ is in dimensionless units, counts per frequency bin.

eccentric orbits. For IMBHs with $m = 10^3 M_\odot$, $t_d \sim 10$ Gyr, and $e = 0.9$, the corresponding cutoff frequency is around 2×10^{-7} Hz = (60 day)⁻¹. *Sources outside the loss cone are in the PTA GW frequency band.*

3.5. Frequency evolution

The above treatment is valid only if the frequency shift is negligible during the observation, which we discuss next.

The timescale on which the GW frequency evolves, is $f/\dot{f} \sim t_d$, where t_d is the timescale on which sources drift inwards. The frequency drift is then $\dot{f}T \sim fT/t_d$. Compared to the frequency resolution $\Delta f = 1/T$ during the observation,

$$\frac{\dot{f}T}{\Delta f} \sim \frac{fT^2}{t_d} \sim 3 \times 10^{-8} f_8 T_{10}^2 t_{d,9}. \quad (15)$$

The frequency drift is negligible due to GW emission or two-body relaxation for sources outside the loss cone.

4. GRAVITATIONAL WAVES AND PULSAR TIMING

The cosmological GW background and its detectability with PTAs can be summarized as follows.

4.1. Stochastic cosmological background

The cosmological GW background constitutes an astrophysical noise for measuring the GWs of objects orbiting SgrA* in the GC. At these frequencies the stochastic GW background is expected to be dominated by SMBH binary inspirals, with a characteristic amplitude roughly (Kocsis & Sesana 2011)

$$h_{c,s} = 1.8 \times 10^{-15} f_8^{-2/3}. \quad (16)$$

The GW background may be suppressed below the stochastic level of Eq. (16) by a factor 2–4 due to gas effects at $f_8 < 1$ (Kocsis & Sesana 2011), and because of small number statistics at $f_8 > 1$ (Sesana et al. 2008). On the other hand, individual cosmological SMBH binary sources may stick out above this background by chance if they happen to be very massive and relatively close-by (Sesana et al. 2009).

4.2. Sensitivity level of PTAs

If pulsars are observed repeatedly in Δt time intervals for a total time T , the spectral resolution is $\Delta f = 1/T$, and the observable frequency range is $1/T \leq f \leq 2/\Delta t$. For $T = 10$ yr, $\Delta t = 1$ week, therefore 3×10^{-9} Hz $\leq f \leq 3 \times 10^{-6}$ Hz.

To derive the angular sensitivity of PTAs, let the unit binary orbit normal, the vectors pointing from the Earth toward the pulsar, and from the binary to the pulsar be respectively, $\hat{L}^a = (\sin \iota \cos \lambda, \sin \iota \sin \lambda, \cos \iota)$, $\hat{p}^a = (\sin \mu \cos \psi, \sin \mu \sin \psi, \cos \mu)$ and $\hat{k}^a = (0, 0, 1)$. In the far-field radiation zone of a circular binary, the metric perturbation is $h_{ab} = h_{ab}^+(t) + h_{ab}^\times(t)$, where

$$h_{ab}^+(t) = 2[1 + (L^c k_c)^2] \mathcal{A} \sin \Phi(t) e_{ab}^\times, \quad (17)$$

$$h_{ab}^\times(t) = 4L^c k_c \mathcal{A} \cos \Phi(t) e_{ab}^+, \quad (18)$$

where \hat{k}_b gives the GW propagation direction, $\Phi(t) = 2\pi f t$ is the GW phase, and $\mathcal{A} = M_\bullet m_*/(Dr)$ is the GW strain amplitude without constant prefactors, which we assume is much larger at the pulsar than at the Earth. Note that D is the distance between M_\bullet and the pulsar, while r is the distance between M_\bullet and m_* . We orient the coordinate system so that $e_{ab}^\times = \hat{e}_a^x \hat{e}_b^y - \hat{e}_b^x \hat{e}_a^y$ and $e_{ab}^+ = \hat{e}_a^x \hat{e}_b^x - \hat{e}_a^y \hat{e}_b^y$ with $\hat{e}_a^x = (1, 0, 0)$,

$\hat{e}_a^y = (0, 1, 0)$. Assuming that the pulsar is much closer to the source than the Earth, the TOAs of pulses change as

$$\delta t = \int z(t) dt, \quad (19)$$

where $z(t) \equiv [\nu(t) - \nu_0]/\nu_0 = z_+(t) + z_\times(t)$, where $\nu(t)$ is the observed pulsar frequency, ν_0 is its unperturbed value (i.e. neglecting GWs), and

$$z_+ = \frac{1}{2} \frac{\hat{p}^a \hat{p}^b}{1 + \hat{p}^a k_a} h_{ab}^+ = (1 - \cos \mu) \cos 2\psi (1 + \cos^2 \iota) \mathcal{A} \cos \Phi \quad (20)$$

$$z_\times = \frac{1}{2} \frac{\hat{p}^a \hat{p}^b}{1 + \hat{p}^a k_a} h_{ab}^\times = (1 - \cos \mu) \sin 2\psi (2 \cos \iota) \mathcal{A} \sin \Phi \quad (21)$$

(Detweiler 1979; Finn 2009; Cornish 2009). Note that unlike for cosmological sources the Earth-term is not included because it is negligible in the timing residual for nearby pulsars. Averaging the redshift factor over an isotropic distribution of \hat{p}_a and \hat{L}_a , and over one GW cycle,

$$z_{\text{GW}} \equiv \sqrt{\langle z_+^2 \rangle + \langle z_\times^2 \rangle} = \frac{4}{\sqrt{15}} \frac{M_\bullet m_\star}{D r(f)} = \frac{1}{\sqrt{6}} h_0(f), \quad (22)$$

where $h_0(f)$ is the RMS GW strain defined in Eq. (5). The variations in the TOAs are given by the integrated change, $z_{\text{GW}}/2\pi f$. For an observation time T , the sensitivity increases with the number of observed cycles as $(fT)^{1/2}$,

$$\delta t_{\text{GW}} = \frac{z_{\text{GW}}}{2\pi f} (fT)^{1/2} = \frac{1}{\sqrt{6}} \frac{h_c(f)}{2\pi f} = 100 m_3 D_{\text{pc}}^{-1} T_{10}^{1/2} f_8^{1/6} \text{ ns}. \quad (23)$$

Thus, instead of the integrated strain $h/(2\pi f)$, the timing SNR is proportional to $h_c/(2\pi f)$, which incorporates the $(fT)^{1/2}$ factor. In the last equality, we assumed the contribution of a single source only, Eq. (13), but in general h_c can represent many sources per bin, given by Eq. (8). Conversely, for fixed δt timing accuracy, the detectable characteristic GW amplitude for an average binary orientation and pulsar direction, is

$$h_{c,\text{PTA}}(f) = \sqrt{6} (2\pi f) \delta t = 1.1 \times 10^{-17} \delta t_{10} f_8, \quad (24)$$

independent of T , where $\delta t_{10} = \delta t/10 \text{ ns}$. The sensitivity is better in certain orientations: by an average factor $\sqrt{3}$ if the binary-pulsar-Earth angle is 90° (with random binary inclination), by $\sqrt{5/2}$ if the pulsar is on the binary orbital axis (with random pulsar-Earth direction), and by $\sqrt{3} \times \sqrt{5/2} = 2.7$ if both conditions hold.

As of 2009, 13 pulsars were known with timing accuracy better than $\delta t \sim 250 \text{ ns}$, the best ones reaching 20–30 ns (Hobbs et al. 2010). The huge collecting area of the future Square Kilometer Array (SKA) implies that it will be able to time many hundreds of pulsars at the level currently achieved for a few pulsars, and will perhaps find ones with much better characteristics (see also Jenet et al. 2009). However, the timing accuracy may be much worse for fainter sources further away (see § 6 below).

4.3. Near-field effects

Up to this point, we assumed that the pulsar signal is modulated by the leading order radiative GW terms, and neglected other post-Newtonian near-field effects. This is justified if the

binary to pulsar distance is $D_p \gg \lambda$, where

$$\lambda = \frac{1}{2\pi f} = 0.16 f_8^{-1} \text{ pc}. \quad (25)$$

is the reduced GW wavelength. Thus, near-field effects will be negligible for $f_8 > 1$ for $D_p \gtrsim 1 \text{ pc}$, but they are significant at lower frequencies for pulsars closer to the center.

Let us estimate the order-of-magnitude of the leading order near-field corrections for the particular geometry of this problem. The variations in the TOAs are approximately determined by the metric $g_{\mu\nu}$ at the pulsar. The near-zone metric induces a variation in the pulsar position and velocity, and modulates the propagation of pulses (Jenet et al. 2005). We resort to simple order-of-magnitude estimates neglecting possibly important lensing effects (Wex et al. 1996; Finn 2009). In the post-Newtonian (PN) approximation, the metric is practically a power series in m_i/r_j , r_i/r_j , and v_i , where m_i are the masses (i.e. M_\bullet or m_\star), and r_j are distance parameters (i.e. r or D), and v_i are the velocities (Blanchet et al. 1998; Alvi 2000; Johnson-McDaniel et al. 2009). The constant coefficients in this power series are typically order 1. We look for periodically varying terms in the 2PN metric of the binary which might be comparable to $h_0(f)$ at the pulsar, and assume the corresponding correction to the gravitational redshift and Doppler shift, collectively called Einstein delay, is proportional to these terms.

For this estimate we restrict to circular binary orbits, where $m_\star \ll M_\bullet \ll r \ll D$, with $m_\star \sim 10^3 M_\odot$, $r \sim \text{mpc}$, $D \sim \text{pc}$. In this regime,

$$\begin{aligned} \frac{r}{D} &\sim 2.6 \times 10^{-3} f_8^{2/3} D_{\text{pc}}^{-1}, & v &\sim \sqrt{\frac{M_\bullet}{r}} = 8.5 \times 10^{-3} f_8^{1/3}, \\ \frac{m_\star}{r} &\ll \frac{M_\bullet}{D} \ll \frac{M_\bullet}{r} \sim 7.3 \times 10^{-5} f_8^{2/3}. \end{aligned} \quad (26)$$

We are not interested in terms that are not time-varying such as M_\bullet/D or M_\bullet^2/D^2 , since these generate a constant gravitational redshift. Remarkably, the mass dipole terms $m_\star r_\star/D^2$ and $M_\bullet r_\bullet/D^2$ are much larger than the standard radiative term $m_\star M_\bullet/rD$ at these distances, but these terms cancel out in the center of mass frame and are not present in the metric. (Here $\mathbf{r}_\bullet = M_\bullet \mathbf{r}/(M_\bullet + m_\star)$ and $\mathbf{r}_\star = m_\star \mathbf{r}/(M_\bullet + m_\star)$ give the vectors to the binary components relative to the barycenter, \mathbf{r} is the binary separation, \mathbf{D} is a field point.) However, the pulsar perceives the binary components at their retarded positions and so the dipole terms do not cancel out exactly unless the binary line-of-sight velocity is zero. The current dipole terms $m_\star(\mathbf{v}_\star \cdot \hat{\mathbf{k}})(\mathbf{r}_\star \cdot \hat{\mathbf{k}})D^{-2}$ are indeed present in the g_{00} , g_{0i} , and g_{ii} components of the binary metric, (see Eq. (2.15) in Alvi 2000; and Eq. (6.4) in Johnson-McDaniel et al. 2009). This leads to an orientation-averaged TOA correction

$$\delta t_{\text{cd}} \sim \frac{m_\star v r}{D^2} \frac{\sqrt{fT}}{2\pi f} = 30 m_3 D_{\text{pc}}^{-2} f_8^{-5/6} T_{10}^{1/2} \text{ ns}. \quad (27)$$

The next correction is the mass quadrupole,

$$\delta t_{\text{mq}} \sim \frac{m_\star r^2}{D^3} \frac{\sqrt{fT}}{2\pi f} = 9 m_3 D_{\text{pc}}^{-3} f_8^{-11/6} T_{10}^{1/2} \text{ ns} \quad (28)$$

Now consider terms higher order in the masses. The leading order term here is the quadrupolar radiation term $M_\bullet m_\star/(Dr) \sim m_\star v^2/D$. which leads to TOA residuals δt_{GW}

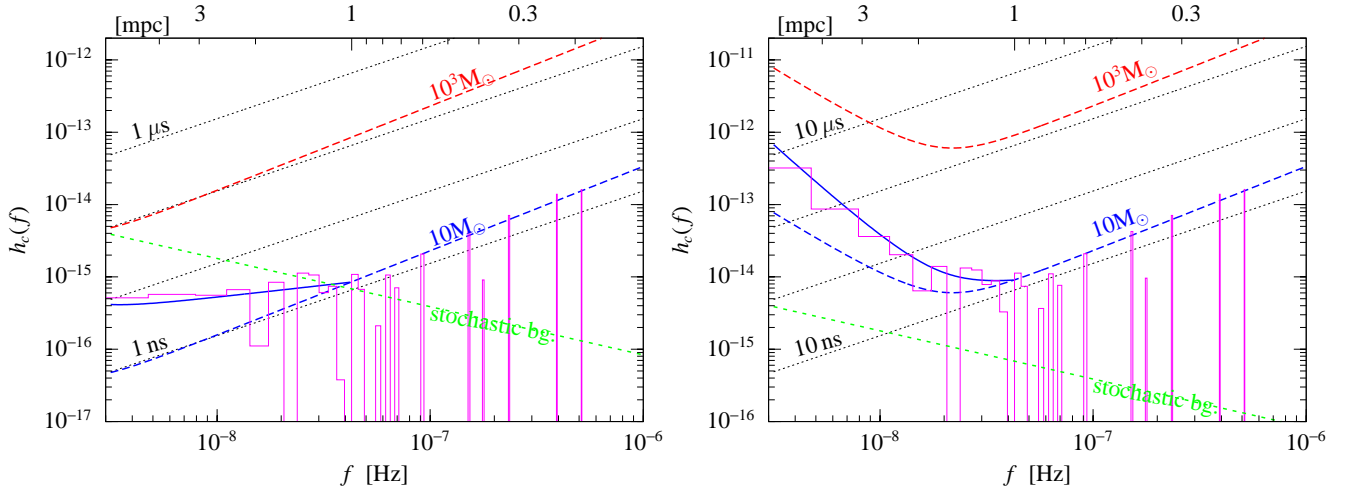


FIG. 1.— The characteristic strain amplitude h_c vs. GW frequency f for a pulsar at 1 pc (left) and 0.1 pc (right) from the Galactic Center. Dotted black lines show the orientation-averaged h_c for fixed timing residuals. Blue and red dashed lines show respectively the orientation-averaged timing residuals caused by individual stellar BHs and IMBHs on circular orbits in a 10 yr observation, assuming 1 object per frequency bin. Magenta lines show the timing residuals for a random realization of $10M_\odot$ stellar BHs in the cluster (20,000 BHs within 1 pc with number density $\propto r^{-2}$). Typically only few bins are occupied at high f , generating a spiky signal with distinct sources. At lower f , many sources overlap to create a continuous spectrum. The RMS average over many realization of the cluster is shown by solid blue. The cosmological RMS stochastic GW background (green dashed) can be much smaller.

of Eq. (23). All other terms in the metric are smaller by positive integer powers of the small parameters in Eq. (26).

In addition to the Einstein delay discussed above, the tidal effects of the binary also induces epicyclic motion in the pulsar, which leads to variations in the path length to Earth. This leads to a timing variation, δt_R , analogous to the Roemer delay in pulsar binaries relative to the binary barycenter. We estimate r_p , the radius of the pulsar’s epicyclic motion around the guiding center of its mean motion. We assume that the pulsar exhibits oscillations on the forcing period, so that its angular velocity matches the angular frequency of the forcing, ω . The centripetal acceleration is then $r_p\omega^2$. We consider the case where the forcing is due to a current dipole or a mass quadrupole, $|F_{cd,R}|/m_p \sim m_*vr \sin \iota / D^3$ and $|F_{mq,R}|/m_p \sim m_*r^2 \sin \iota / D^4$. The time lag is $\delta t_R \sim 2r_p \cos \mu$ in a half cycle, and we assume the measurement improves with $(fT)^{1/2}$ for longer observations. Neglecting factors of order unity, we get

$$\delta t_{cd,R} \sim \frac{m_*vr}{D^3} \frac{\sqrt{fT}}{(2\pi f)^2} = 5m_3 D_{pc}^{-3} f_8^{-11/6} T_{10}^{1/2} \text{ ns}, \quad (29)$$

$$\delta t_{mq,R} \sim \frac{m_*r^2}{D^4} \frac{\sqrt{fT}}{(2\pi f)^2} = 1m_3 D_{pc}^{-4} f_8^{-17/6} T_{10}^{1/2} \text{ ns}. \quad (30)$$

These estimates are consistent with that of Jenet et al. (2005). They found timing residuals corresponding to $\delta t_{mq,R}$ can be 500ns for a pulsar inside a globular cluster with $D_{pc} = 0.03$, $f_8 = 0.3$, $T_{10} = 1$ for a $10M_\odot$ BH orbiting around an 10^3M_\odot IMBH. The residuals are much larger in the near-field zone of the Galactic nucleus where the central object is a SMBH.

In conclusion, the Einstein delay terms δt_{cd} and δt_{mq} given by Eqs. (27–28) are much larger than the Roemer delay $\delta t_{cd,R}$ and $\delta t_{mq,R}$ for $D \gtrsim pc$ and $f > 10\text{ nHz}$. In particular, δt_{cd} is comparable to the standard radiative GW modulation, δt_{GW} at 10nHz. The gravitational near field timing residuals of individual sources become much larger for pulsars at $D \sim 0.1\text{ pc}$, at the level $\delta t_{cd} \sim \delta t_{mq,R} \sim 10m_3 \mu\text{s}$ at $f \sim 10m_3 \text{ nHz}$, and even larger for smaller f . For stellar mass BHs, the individual contributions of residuals are overlapping in Fourier space where near-field effects are most important (see Eq. (10)),

and the net timing residual can be estimated by scaling with $\sqrt{dN/d \ln f}$ using Eq. (8).

5. RESULTS

We can now combine the results above to draw conclusions on the detectability of GWs from the GC with pulsars in its neighborhood. From Eq. (23), the distance within which a PTA could measure the GWs of an individual source with a fixed timing precision $\delta t = 10\delta t_{10\text{ ns}}$ is

$$D_{\delta t} = 14m_3 \delta t_{10}^{-1} T_{10}^{1/2} f_8^{1/6} \text{ pc}. \quad (31)$$

Eqs. (13) and (16) show that the GWs from an individual BH in the GCs rises above the stochastic GW background within a distance

$$D_{bg} = 8.7m_3 T_{10}^{1/2} f_8^{11/6} \text{ pc}. \quad (32)$$

A pulsar within $D_{\delta t}$ and D_{bg} to the GC could be used to detect GWs from individual objects in the GC. These estimates are conservative. First, they assume an average orbital and pulsar orientation, D_b and $D_{\delta t}$ might be 2–3 \times larger for certain orientations. Second, Eq. (32) assumes that small number statistics and gas effects are negligible in cosmological SMBH mergers, and might overestimate the background (Sesana et al. 2008; Kocsis & Sesana 2011).⁴

Figure 1 shows the orientation averaged characteristic GW amplitude for a 10 year observation, incorporating the additional near-field effects using Eqs. (24) and (27–30). The lower and top x -axis shows the GW frequency and orbital radius for circular sources. The magenta curve displays the spectrum of timing residuals for a Monte Carlo realization of a population of 20,000 BHs within 1 pc with number density $n(r) \propto r^{-2}$ and random orientation with mass $10M_\odot$ on circular orbits. The solid blue line shows the RMS foreground of a cusp of stellar mass BH averaged over different realizations. The spectrum separates into distinct spectral spikes at higher frequencies with RMS maxima shown by the dashed line. Figure 2 shows the GW amplitude of a realization

⁴ Note that the signal from individual cosmological SMBHs can also be enhanced by a factor 2–3 for certain orientations, but this effect is washed out for the unresolved stochastic background.

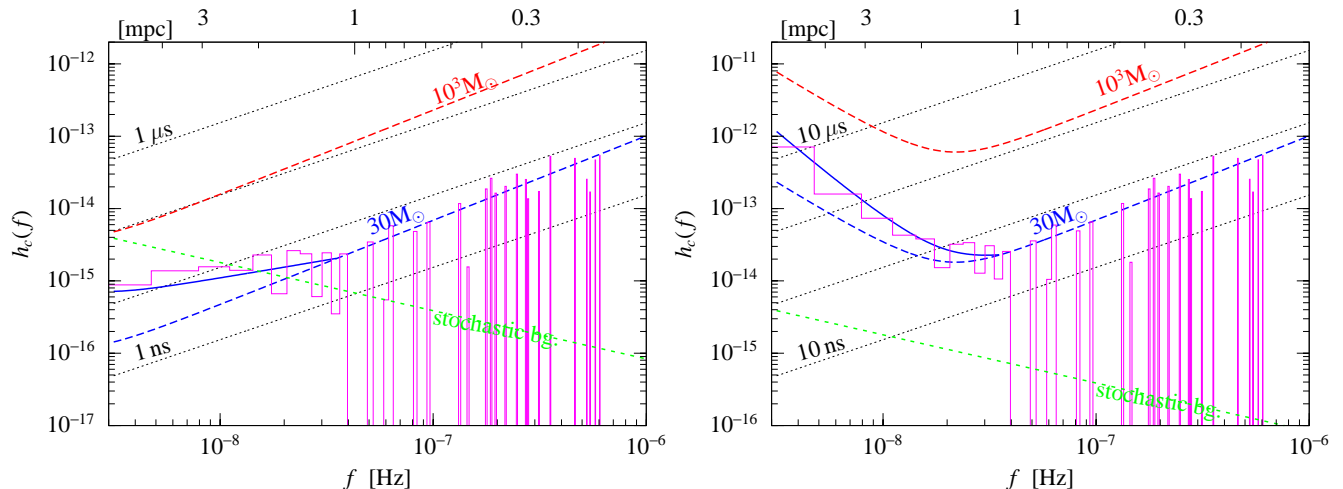


FIG. 2.— Same as Fig. 1 but for 1000 BHs of mass $30M_{\odot}$ within 1 pc, with a steeper density profile $r^{-2.5}$. There are more resolvable sources in this case.

of 1000 BHs with mass $30M_{\odot}$ in 1 pc with a steeper number density profile $n(r) \propto r^{-2.5}$. Despite of the smaller overall number of sources in the cluster, there are many more resolvable sources within 1 mpc in this case.

The net background level in Figures 1 and 2 is conservative, as the background is sensitive to the RMS mass of objects in the cluster, which may significantly exceed the mean. Furthermore, individual sources may generate up to $\sim 3\times$ larger timing residuals for certain orientations. Timing pulsars at a distance 0.1–1 pc from the Galactic Center with 100ns – $10\mu\text{s}$ timing precision can be used to detect IMBHs of mass 10^3M_{\odot} , if they exist within 6 mpc of SgrA*. A population of stellar BHs within 2–5 mpc generates timing variations greater than 100ns – $10\mu\text{s}$ for a pulsar within 0.1 pc. However it will be much more difficult to individually resolve $10M_{\odot}$ stellar BHs within 1 mpc to SgrA*, which requires an extreme 1–20 ns timing precision.

Figure 3 shows the characteristic GW spectra for a Monte Carlo realization of an eccentric population of $10M_{\odot}$ BHs with an isotropic thermal eccentricity distribution. Magenta and cyan lines show the contribution of periodic and burst sources, respectively. The dashed lines show $h_c(f)$ for individual circular sources, and the solid blue lines represent the RMS GW level for a population of circular sources for comparison. The net GW spectrum of burst sources is typically less than the level of periodic sources. The figure verifies the analytical calculations of Appendix A, the continuous low-frequency spectrum of periodic sources is indeed comparable to the circular level, modulo a weakly frequency dependent constant between $0.4 \lesssim K \lesssim 0.8$. Note that for clarity, we are not including the gravitational near field effects here, which would dominate over the continuous low-frequency GW spectrum for $D \sim 0.1$ pc as shown in Figure 1.

The transition to a spiky spectra happens at somewhat larger frequencies for eccentric sources (c.f. Figs. 1 and 3). Since individual sources generate GW spectra with many orbital upper harmonics, the net high frequency spectrum is more complicated than in the circular case. The orientation averaged spectral level for individual sources is typically less than $\delta t \lesssim 200\text{ns}m_3D_{\text{pc}}^{-1}$ per frequency bin, however, the total root-sum-squared signal of all upper harmonics of individual sources is much larger than the level of a single bin. In Appendix A we show that the SNR for detecting individual sources with a matched filter is comparable for eccentric

and circular sources. In this sense, the dashed lines in Fig. 3, are representative of the total timing residual of individual sources as a function of pericenter frequency for arbitrary eccentricity. However, the full spectrum is rich in narrow features for eccentric sources and pericenter precession slowly modulates the amplitude of the timing residuals in individual pulsars. Both of these features could help to separate individual eccentric sources from the signal of other sources in GC.

6. DISCUSSION

We have shown that pulsars within a few pc distance from the GC offer a unique probe to identify IMBHs and stellar BHs orbiting around SgrA*. An IMBH, if present in the GC, sinks to orbital radii corresponding to the pulsar timing frequency bands. Depending on the binary orientation, orbital frequency, and pulsar distance, the GWs and gravitational near-field effects modulate the TOAs by a few ns to $100\mu\text{s}$ for these sources with masses between $10M_{\odot}$ and 10^4M_{\odot} . Based on the GW spectral features, the signals of more than one IMBH (up to tens, if present) could be individually resolved and isolated from the fainter signal of stars and stellar mass objects and the cosmological GW background.

This observational probe is complimentary to EM measurements with different systematics. GWs are generated by all gravitating objects, including those that are black and undetectable in EM bands. GWs escape the galactic nucleus without any dissipation or dispersion. Closer to SgrA*, sources generate stronger, higher frequency GWs, the number of observable cycles increases, and the number of objects per frequency bin decreases. Thus, unlike EM imaging techniques, the prospects for detecting and resolving individual objects through GW measurements improve closer in towards SgrA*, even if the number density of objects increases inwards steeply. Furthermore, the gravitational effects are proportional to the RMS mass of objects, making the measurement more sensitive to individual higher mass objects in the distribution, even if the total mass of lighter objects is somewhat larger on comparable radius orbits.

Repeated pulsar timing observations over a few year baseline could reveal a detailed census of BHs in the inner mpc of the GC. We have shown that the GW foreground of stellar BHs rises above the cosmological background and separates into distinct peaks above 40 nHz, corresponding to a GW period of less than 1 yr or orbital separations less than

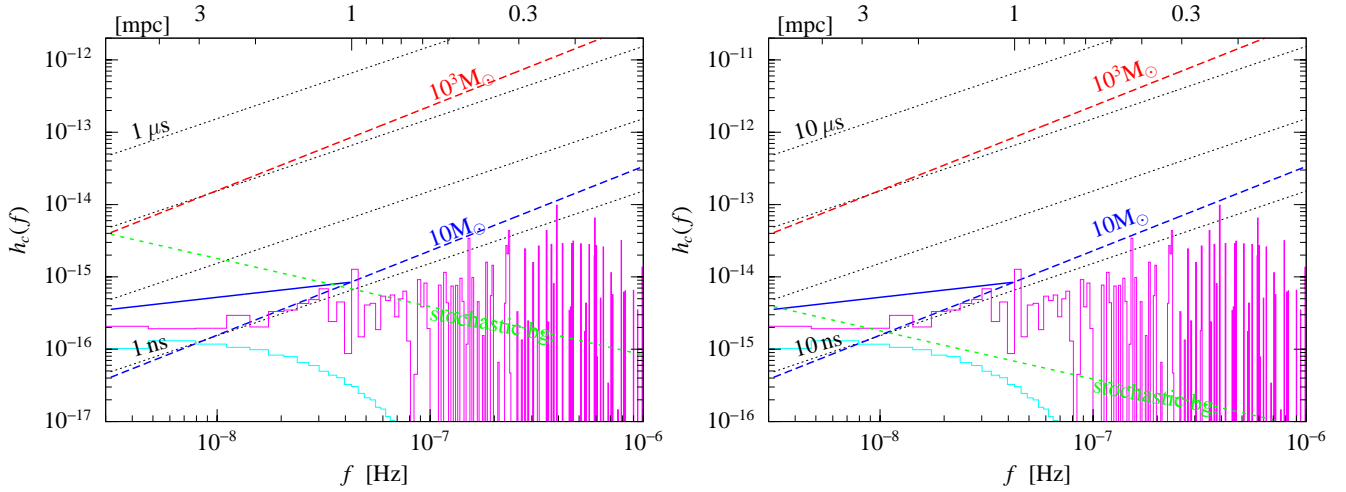


FIG. 3.— Characteristic spectral amplitude $h_c(f)$ for timing a pulsar at 1 pc (left) and 0.1 pc (right) from the GC for a population of $10M_\odot$ BHs with isotropic thermal eccentricity distribution. The contribution of periodic sources are shown with magenta, burst sources with cyan. For comparison, the dashed blue and red lines show the RMS GW level for individual circular sources, and solid blue lines show the RMS level from a population of circular $10M_\odot$ sources (see sections 2.1 and 2.2). Note that timing variations due to gravitational near field effects are not shown, which dominate within 3×10^{-8} Hz (see Figures 1 and 2).

1 mpc. Based on a simple estimate using circular orbits, we found that the total number of individually resolvable BHs is between 7–70, depending on the radial number density distribution exponent $r^{-\alpha}$ between $r^{-1.75}$ and $r^{-2.25}$. These observations are therefore exponentially sensitive to α , capable of testing the theory of strong mass segregation (Keshet et al. 2009).

Eccentricity complicates the spectral shape of resolvable sources by adding upper frequency harmonics. Although the timing residuals in individual frequency bins is suppressed by this effect relative to circular orbits, the total timing residual SNR with a matched filter is comparable for eccentric sources. At lower frequencies, a population of objects on eccentric orbits generates a stochastic GW foreground with a similar spectral shape and a comparable amplitude, as a circular population. Objects on larger-semimajor axis, eccentric orbits generate GW bursts during pericentric passage near SgrA*. The stochastic GW burst signal is much less than the level of periodic sources.

This analysis hinges on the assumption that future surveys will discover pulsars near the GC that can be timed to the sufficient accuracy. Most of the observed S-stars within a few mpc and the young O/B stars in the GC will eventually turn into pulsars in a supernova explosion (Pfahl & Loeb 2004). Based on the age and number of these stars, and assuming that we don’t live in a special time, one might expect more than 10^4 pulsars in the GC. Some of these may become MSPs, and may be beamed towards us to be detectable with future SKA-type instruments (Cordes et al. 2004). They might be expected to segregate to the outskirts of the GC on a Gyr timescale as heavier objects sink inwards (Chanamé & Gould 2002). Recently, Liu et al. (2012) examined the expected timing accuracy of pulsars in the GC accounting for radiometer noise, pulse phase jitter, and the interstellar scintillation of the ISM. They found that the 1 hr timing accuracy of SKA is expected to be between 10–100 μs for regular pulsars. Our results indicate that the necessary accuracy to detect timing variations associated to individual $10M_\odot$ BHs within 1 mpc requires much higher timing accuracy, which might be prohibitively difficult even with MSPs with a factor of 100–1000 better timing accuracy. However, the net variations caused by a population of these objects is detectable between 2–5

mpc at these accuracy levels. Remarkably, a 10–100 μs timing accuracy is sufficient to individually resolve or rule out the existence of $10^3 M_\odot$ IMBHs within 5 mpc from SgrA*.

As the GW spectrum is rich in strong spiky features at high frequencies, it may be possible to isolate GW induced timing residuals from other systematic effects. One such effect is if the pulsar itself is a part of a binary system. Fortunately, however, binaries with orbital periods of years, matching the GW foreground of the GC, are very soft, and are not long lived near the GC, they are easily disrupted by three-body encounters. Indeed, due to the high velocity dispersion in the GC, $\sigma \sim 200 \text{ km/s}$ at $D \sim \text{pc}$, stellar mass binaries are soft for orbital frequencies $f \lesssim (2\pi)^{-1} \sigma^3 / (GM_\odot) \sim 9,600 \text{ nHz}$, or orbital period $f^{-1} \gtrsim 1.2 \text{ day}$. The evaporation timescale on which a series of more distant encounters gradually increases the binary separation, is $t_e \sim 0.06 \sigma / (G\rho a \ln \Lambda) \sim 40 f_8^{2/3} \text{ Myr}$, where Λ is the Coulomb logarithm, and the ionization timescale to disrupt the binary by a close three body encounter is $t_i \sim 0.04 \sigma / (G\rho a) \sim 70 f_8^{2/3} \text{ Myr}$ (see § 7.5.7. in Binney & Tremaine 2008). Here we have expressed the binary semimajor axis a with the orbital frequency, which is of order $0.1 \lesssim f_8 \lesssim 10$ to match the GW signal. Thus, MSPs which form in short period binaries, like in typical LMXBs, and become wide, may be expected to typically become single in the GC. However, a few pulsar-BH binaries may form through three body exchange interactions and may be longer lived in the GC (Faucher-Giguère & Loeb 2011). Ultimately, multiple pulsars would be necessary to rule out systematic effects.

GW observations with pulsar timing in the GC could be combined with other observable channels to map the GC. An IMBH orbiting around the SMBH would be observable with future millimeter VLBI imaging with EHT (Broderick et al. 2011). Conversely, if those observations reveal an IMBH, the inferred orbital parameters could help in identifying the GW counterpart with pulsar timing.

BK acknowledges support from NASA through Einstein Postdoctoral Fellowship Award Number PF9-00063 issued by the Chandra X-ray Observatory Center, which is operated by the Smithsonian Astrophysical Observatory for and on behalf

of the National Aeronautics Space Administration under contract NAS8-03060. AR thanks the Director and members of the Institute for Theory and Computation (ITC), Harvard University for hospitality. He also thanks Woldek Kluzniak, Duncan Lorimer and Maura McLaughlin for discussions. This work was supported by the Hungarian Research Fund OTKA

(grant 68228), Netherlands Research Council NWO (grants #639.073.803), the Netherlands Research School for Astronomy (NOVA), the Eleventh Five Year Plan Project No. 11P-409 at Tata Institute of Fundamental Research (TIFR) and by a Visiting Scholarship at the ITC.

APPENDIX ECCENTRIC SOURCES

Here we present the mathematical derivation of the GW foreground of eccentric sources in the GC. We start by reviewing the eccentric waveforms and GW spectra, then calculate the GW background of an eccentric population of periodic sources and burst sources, respectively, and finally discuss simple estimates of the signal-to-noise ratio of timing residuals for individual eccentric sources.

Waveform

An individual eccentric source with semimajor axis a and eccentricity e , generates a GW strain composed of discrete upper harmonics with frequency $f_n = n f_{\text{orb}}$,

$$h(a, e, t) = \sum_{n=1}^{\infty} h_n(a, e; f_n) e^{2\pi i f_n t} \quad (\text{A1})$$

where

$$h_n(a, e; f_n) = \frac{2}{n} \sqrt{g(n, e)} h_0(a), \quad (\text{A2})$$

where $h_0(a) = \sqrt{32/5} M_{\bullet} m_{\star} / (Da)$ is the GW strain amplitude for circular orbits, and

$$g(n, e) = \frac{n^4}{32} \left[\left(J_{n-2} - 2eJ_{n-1} + \frac{2}{n} J_n + 2eJ_{n+1} - J_{n+1} \right)^2 + (1-e^2)(J_{n-2} - 2J_n + J_{n+2})^2 + \frac{4}{3n^2} J_n^2 \right]. \quad (\text{A3})$$

Here $J_i \equiv J_i(x)$ is the i th Bessel function evaluated at $x = ne$ (Peters & Mathews 1963), and we have RMS averaged over the binary inclination. The Fourier transform of $h(a, e, t)$ measured for some time T is then

$$\tilde{h}(a, e, f) = \sum_{n=1}^{\infty} h_n(a, e; f_n) T w(f, f_n, T), \quad \text{where } w(f, f_n, T) = \frac{\sin[2\pi(f - f_n)T]}{2\pi(f - f_n)T}. \quad (\text{A4})$$

Here $w(f, f_n, T)$ is the Fourier transform of a window function of width T and a unit integral. It approaches unity at $f = f_n$ and cuts off for $|f - f_n| \gtrsim 1/2T$. The spectral width of each GW harmonic is $\Delta f \sim 1/T$.

For circular sources, $g(n, 0) = 1$ for $n = 2$ and 0 otherwise. For eccentric sources, the dominant frequency harmonic is $f_p = n_p f_{\text{orb}}$, the inverse pericenter passage timescale,

$$n_p(e) = \text{ceil} \left[1.15 \frac{(1+e)^{1/2}}{(1-e)^{3/2}} \right], \quad \text{so that } f_p(a, e) \sim \frac{(1+e)^{1/2}}{(1-e)^{3/2}} f_{\text{orb}}(a), \quad (\text{A5})$$

where $\text{ceil}(x)$ is the nearest integer larger than x (O'Leary et al. 2009). The emitted GW spectrum is broadband with a maximum near f_p , where 90% and 99% of the power is between $0.2 f_p < f < 3 f_p$ and between $0.1 f_p < f < 5 f_p$, respectively. The $g(n, e)$ harmonic weights in Eq. (A3) have a maximum near $n_p(e)$.

The definition of the inclination-averaged GW strain amplitude (A2) can be made more lucid by recalling the definition of the GW flux, $S = \dot{h}(t)^2 / 16\pi$, and verify if the total power output is consistent with Eq. (16) of Peters & Mathews (1963). Indeed,

$$P = 4\pi D^2 S = \frac{1}{4} D^2 \dot{h}^2 = \pi^2 D^2 \sum_{n=1}^{\infty} n^2 f_{\text{orb}}^2 h_n^2 = 4\pi^2 D^2 f_{\text{orb}}^2 h_0^2 F(e) = \frac{32 M_{\bullet}^3 m_{\star}^2}{5 a^5} F(e) \quad (\text{A6})$$

where we have used Kepler's law $\omega_{\text{orb}}^2 = 4\pi^2 f_{\text{orb}}^2 = M_{\bullet} / a^3$, the definition of h_0 ,

$$F(e) \equiv \sum_{n=1}^{\infty} g(n, e) = \frac{F_1(e)}{(1-e^2)^{7/2}}, \quad \text{and } F_1(e) = 1 + (73/24)e^2 + (37/39)e^4. \quad (\text{A7})$$

GW background of periodic sources

Let us estimate the net contribution of many sources to the GW background if observed for time T . For a source with semimajor axis a and eccentricity e , the counts in each frequency bin f are given by

$$h_{c,1}^2(a, e; f) = \tilde{h}^2(a, e; f) f \Delta f = \sum_{n=1}^{\infty} f T h_0^2(a) \frac{4}{n^2} g(n, e) \times \begin{cases} 1 & \text{if } |f - f_n(a)| \leq \Delta f / 2 \text{ and } fT > 1 \\ 0 & \text{otherwise} \end{cases}. \quad (\text{A8})$$

where $f_n(a) = n f_{\text{orb}}(a) = n(2\pi M_\bullet)^{-1} (a/M_\bullet)^{-3/2}$ is the GW frequency of the n^{th} upper harmonic for a fixed semimajor axis. Conversely, the range of semimajor axis, $a_n \pm 0.5\Delta a_n$, for which the n^{th} harmonic contributes to the frequency bin between $f \pm 0.5\Delta f$, is

$$a_n = M_\bullet (2\pi M_\bullet f/n)^{-2/3} = \left(\frac{n}{2}\right)^{2/3} a_2. \quad (\text{A9})$$

where $\Delta a_n = |da_n/df| \Delta f = \frac{2}{3} a_n / (fT)$.

Now let us assume a phase space distribution, in which the number of objects in the neighborhood of (a, e) is $d^2N = (\partial^2 N / \partial a \partial e) da de$. The number of sources that contribute to the n^{th} harmonic is $\Delta N_n = \int de (\partial^2 N / \partial a_n \partial e) \Delta a_n$. The GW signal of all sources is then

$$h_{\text{c,per}}^2(f) = \int_0^1 de \sum_{n=1}^{n_{\text{max}}} \left[\left(\frac{\partial^2 N}{\partial a \partial e} \left| \frac{da}{df} \right| \Delta f \right) h_{\text{c},1}^2(a, e; f) \right]_{a=a_n}. \quad (\text{A10})$$

For periodic sources, n_{max} is set by the condition that objects are observed for at least one orbit, $1/f_{\text{orb}}(a_n) = n/f \lesssim 1/T$, implying that $n_{\text{max}} = fT$. We shall consider the contribution of burst sources, on larger radius orbits observed for only a fraction of the orbit, separately below. Rearranging and using Eq. (A8), $(\partial^2 N / \partial a \partial e) = 4\pi a^2 n_\star(a) \varphi(e)$, and $da/df = \frac{2}{3} a/f$, gives

$$h_{\text{c,per}}^2(f) = \sum_{n=1}^{fT} \frac{8\pi}{3} a_n^3 n_\star(a_n) h_0^2(a_n) \int_0^1 de \varphi(e) \frac{4}{n^2} g(n, e). \quad (\text{A11})$$

Let us assume that $n_\star(a) \propto a^{-\alpha}$. Then using $h_0(a) \propto a^{-1}$ and Eq. (A9), we find that the RHS is proportional to $a_n^{1-\alpha}$. Now let us express a_n with a_2 using Eq. (A9),

$$h_{\text{c,per}}^2(f) = \frac{8\pi}{3} a_2^3 n_\star(a_2) h_0^2(a_2) K_{\text{per}}(f) \quad (\text{A12})$$

where

$$K_{\text{per}}(f) = \int_0^1 de \sum_{n=1}^{fT} \left(\frac{2}{n}\right)^{(2+\alpha)2/3} \varphi(e) g(n, e). \quad (\text{A13})$$

Thus $K_{\text{per}}(f) = 0$ at $f \leq 1/T$, and increases monotonically, and asymptotes a constant for $n_{\text{max}} = fT \rightarrow \infty$. One can show⁵ that this constant is insensitive to the highest eccentricity sources if $\alpha > 1/2$, which is expected to be satisfied. For $\alpha = 2$ and a thermal distribution of eccentricities $\varphi(e) = 2e$, we get $K_{\text{per}} \sim 0.8$ for $fT \gg 1$. This together with Eq. (A12) shows that the net GW spectrum of a continuous population of eccentric sources is very similar to that of circular sources. However, the signal is much different for individually resolvable sources, as they are comprised of many upper harmonics

GW background of burst sources

GW bursts are generated by objects which make only one close approach near the SgrA* during the observation. These sources are on eccentric orbits with orbital time f_{orb}^{-1} exceeding T , but for which the pericenter timescale f_p^{-1} is less than T and the orbital phase is such that pericenter passage occurs within the observation. The later condition means that only a $1/(f_p T)$ fraction of all such sources will contribute in the observation time. For a fixed measurement frequency, f , therefore $f_{\text{orb}} = f/n < 1/T$, $f n_p/n > 1/T$. Therefore $fT < n < n_p fT$ and the fraction among these sources that contribute is $n/(n_p fT)$.

Repeating the derivation for the net GW burst background over time T , Eq. (A8–A10), we get

$$h_{\text{c,b}}^2(f) = \frac{8\pi}{3} a_2^3 n_\star(a_2) h_0^2(a_2) K_b(f) \quad (\text{A14})$$

where

$$K_b(f) = \int_{e_{\text{min}}}^1 de \sum_{n=fT}^{n_p fT} \frac{n}{n_p fT} \left(\frac{2}{n}\right)^{(2+\alpha)2/3} \varphi(e) g(n, e). \quad (\text{A15})$$

Note that resolving the burst source also requires that the sampling frequency $f_{\text{max}} = 2/\Delta t$ and timescale between observations Δt to satisfy $f_p \lesssim f_{\text{max}}$ and $\Delta t/2 \lesssim f_p^{-1}$. This implies that $n_{\text{min}} \gtrsim \frac{1}{2} n_p f \Delta t$ has to hold. This requirement, however, is typically already satisfied for most sources if $\Delta t \gtrsim 1$ week, the number of sources on so eccentric orbits with such small r_p , is close to zero. Comparing $K_{\text{per}}(f)$ and $K_b(f)$, Eqs. (A13) and (A15), shows that the net GW signal of periodic sources exceeds the contribution of GW burst sources.

⁵ To see this, consider an approximate sharply peaked signal around f_p , for which $g(n, e) \sim \delta_{n, n_p(e)} F(e)$, where $\delta_{ij} = 1$ if $i = j$ and 0 otherwise.

Signal to noise ratio

Here we present simple estimates on the scaling of the GW signal and timing SNR for eccentric sources using elementary functions. This is useful not only because the exact signal presented above is algebraically complicated, but also because the total SNR for individual sources is not represented well by $h_c(f)$ in a single frequency bin, but it is sensitive to the coherent sum over many orbital harmonics.

Let us define an effective GW strain amplitude using that the GW power at pericenter passage, P_p , is the average power times the fraction of time the source spends near pericenter passage, i.e. n_p , given by Eq. (A5). Thus,

$$P_p = \frac{1}{4} D^2 \omega_p^2 h_p^2 = n_p P = \frac{32}{5} \frac{M_\bullet^3 m_\star^2}{r_p^5} (1+e)^{1/2} F_1(e). \quad (\text{A16})$$

This amounts to the root-sum-square of individual frequency harmonics in the spectrum for single sources, without averaging over the full orbit (c.f. Eq. (A6)). From this we get, that the effective strain at close passage is

$$h_p = 2 \frac{(n_p P)^{1/2}}{D \omega_p} = \sqrt{\frac{32}{5}} 2 \frac{M_\bullet m_\star}{D r_p} F_1^{1/2}(e) \quad (\text{A17})$$

where $\omega_p = 2\pi f_p$ and we have used $\omega_p = M^{1/2}(1+e)^{1/2} r_p^{-3/2}$. The pulsars are sensitive to the time integral of the strain (see § 4.2),

$$\mathcal{H}_c = \frac{h_p}{\omega_p} (f_{\text{orb}} T)^{1/2} = \sqrt{\frac{32}{5}} \frac{1}{\pi} \frac{M_\bullet^{3/4} m_\star}{D a^{1/4}} T^{1/2} \frac{(1-e)^{1/2}}{(1+e)^{1/2}} F_1^{1/2}(e). \quad (\text{A18})$$

The SNR is then $S/N = \mathcal{H}_c / \delta t_0$ where δt_0 is the timing noise over time f_p^{-1} . Note that the RMS of the eccentricity dependent terms is 0.438 in Eq. (A18), if the eccentricity is drawn from a thermal distribution $\varphi(e) = 2e$ between $0 \leq e \leq 1$ (Binney & Tremaine 2008). The SNR of the timing residual is not very sensitive to the semimajor axis, or the maximum eccentricity in the cluster. For fixed a , eccentric sources contribute to the net timing residuals at a similar level as circular sources.

Eq. (A18) is only applicable for periodic sources, i.e. if $f_{\text{orb}} T \geq 1$. For a single GW burst source with $1/f_p < T < 1/f_{\text{orb}}$,

$$\mathcal{H}_{c,\text{lb}} = \frac{h_p}{\omega_p} = \frac{1}{2\pi} \sqrt{\frac{32}{5}} \frac{M_\bullet^{1/2} m_\star}{D} \frac{r_p^{1/2}}{(1+e)^{1/2}} F_1^{1/2}(e), \quad (\text{A19})$$

provided that the orbital phase coincides with pericenter passage during the observation. This shows that for burst sources with fixed pericenter distance, the total timing residual is weakly dependent on eccentricity, for fixed pericenter distance. The number of sources is constant as a function of r_p for fixed e , but the fraction of sources that are near pericenter passage at any given instant decreases quickly for smaller r_p proportional to $1/n_p$. Therefore the net contribution of burst sources scales as

$$\mathcal{H}_{c,\text{b}} = \Delta N \mathcal{H}_{c,\text{lb}} = \mathcal{H}_{c,\text{lb}} (\omega_p T)^{1/2} n_{rp} \Delta r_p = \frac{h_p}{\omega_p} (\omega_p T)^{1/2} n_{rp} \Delta r_p = \frac{1}{\pi} \sqrt{\frac{32}{5}} \frac{M_\bullet^{3/4} m_\star}{D r_p^{1/4}} \frac{T^{1/2} n_{rp} \Delta r_p}{(1+e)^{1/2}} F_1^{1/2}(e) \quad (\text{A20})$$

The spectral density within a frequency bin follows from $\Delta r_p = (2/3) \omega_p^{-5/3} \Delta \omega_p$ implying that $\mathcal{H}_{c,u} \propto r_p^{-1/4} \Delta r_p \propto \omega_p^{-3/2} \Delta \omega_p$. The average timing spectral density of burst sources decreases quickly toward higher frequencies.

REFERENCES

- Alexander, T., & Hopman, C. 2009, ApJ, 697, 1861
 Alvi, K. 2000, Phys. Rev. D, 61, 124013
 Bahcall, J. N., & Wolf, R. A. 1976, ApJ, 209, 214
 Bates, S. D., et al. 2011, MNRAS, 411, 1575
 Baumgardt, H., Gualandris, A., & Portegies Zwart, S. 2006, MNRAS, 372, 174
 Binney, J., & Tremaine, S. 2008, Galactic Dynamics: Second Edition (Princeton University Press)
 Blanchet, L., Faye, G., & Ponsot, B. 1998, Phys. Rev. D, 58, 124002
 Blandford, R. D., Romani, R. W., & Applegate, J. H. 1987, MNRAS, 225, 51P
 Broderick, A. E., Loeb, A., & Reid, M. J. 2011, ApJ, 735, 57
 Chanamé, J., & Gould, A. 2002, ApJ, 571, 320
 Cordes, J. 2007, Pulsar searches and timing with the SKA, <http://www.skatelescope.org/>
 Cordes, J. M., Kramer, M., Lazio, T. J. W., Stappers, B. W., Backer, D. C., & Johnston, S. 2004, New A Rev., 48, 1413
 Cornish, N. J. 2009, Phys. Rev. D, 80, 087101
 Davis, S. W., Narayan, R., Zhu, Y., Barret, D., Farrell, S. A., Godet, O., Servillat, M., & Webb, N. A. 2011, ApJ, 734, 111
 de Paolis, F., Gurzadyan, V. G., & Inghoso, G. 1996, A&A, 315, 396
 Deneva, J. S., Cordes, J. M., & Lazio, T. J. W. 2009, ApJ, 702, L177
 Detweiler, S. 1979, ApJ, 234, 1100
 Faucher-Giguère, C.-A., & Loeb, A. 2011, MNRAS, 911
 Finn, L. S. 2009, Phys. Rev. D, 79, 022002
 Freitag, M., Amaro-Seoane, P., & Kalogera, V. 2006a, ApJ, 649, 91
 Freitag, M., Gürkan, M. A., & Rasio, F. A. 2006b, MNRAS, 368, 141
 Fritz, T. K., et al. 2010, ApJ, 721, 395
 Fujii, M., Iwasawa, M., Funato, Y., & Makino, J. 2009, ApJ, 695, 1421
 Genzel, R., Eisenhauer, F., & Gillessen, S. 2010, Reviews of Modern Physics, 82, 3121
 Gillessen, S., Eisenhauer, F., Trippe, S., Alexander, T., Genzel, R., Martins, F., & Ott, T. 2009, ApJ, 692, 1075
 Gualandris, A., Gillessen, S., & Merritt, D. 2010, MNRAS, 409, 1146
 Gualandris, A., & Merritt, D. 2009, ApJ, 705, 361
 —. 2012, ApJ, 744, 74
 Gualandris, A., Portegies Zwart, S., & Sipior, M. S. 2005, MNRAS, 363, 223
 Hansen, B. M. S., & Milosavljević, M. 2003, ApJ, 593, L77
 Hobbs, G., et al. 2010, Classical and Quantum Gravity, 27, 084013
 Iwasawa, M., An, S., Matsubayashi, T., Funato, Y., & Makino, J. 2011, ApJ, 731, L9
 Jaffe, A. H., & Backer, D. C. 2003, ApJ, 583, 616
 Jenet, F., et al. 2009, arXiv:0909.1058
 Jenet, F. A., Creighton, T., & Lommen, A. 2005, ApJ, 627, L125
 Jenet, F. A., Lommen, A., Larson, S. L., & Wen, L. 2004, ApJ, 606, 799
 Johnson-McDaniel, N. K., Yunes, N., Tichy, W., & Owen, B. J. 2009, Phys. Rev. D, 80, 124039

- Johnston, S., Kramer, M., Lorimer, D. R., Lyne, A. G., McLaughlin, M., Klein, B., & Manchester, R. N. 2006, *MNRAS*, 373, L6
- Keith, M. J., Johnston, S., Levin, L., & Bailes, M. 2011, *MNRAS*, 418, 948
- Keshet, U., Hopman, C., & Alexander, T. 2009, *ApJ*, 698, L64
- Khan, F. M., Just, A., & Merritt, D. 2011, *ApJ*, 732, 89
- Kocsis, B., & Levin, J. 2011, arXiv:1109.4170
- Kocsis, B., & Sesana, A. 2011, *MNRAS*, 411, 1467
- Königsdörffer, C., & Gopakumar, A. 2006, *Phys. Rev. D*, 73, 124012
- Kramer, M., Xilouris, K. M., Lorimer, D. R., Doroshenko, O., Jessner, A., Wielebinski, R., Wolszczan, A., & Camilo, F. 1998, *ApJ*, 501, 270
- Lazio, T. J. W., & Cordes, J. M. 1998, *ApJ*, 505, 715
- Liu, K., Wex, N., Kramer, M., Cordes, J. M., & Lazio, T. J. W. 2012, *ApJ*, 747, 1
- Lommen, A. N., & Backer, D. C. 2001, *ApJ*, 562, 297
- Macquart, J.-P., Kanekar, N., Frail, D. A., & Ransom, S. M. 2010, *ApJ*, 715, 939
- Madau, P., & Rees, M. J. 2001, *ApJ*, 551, L27
- Maillard, J. P., Paumard, T., Stolovy, S. R., & Rigaut, F. 2004, *A&A*, 423, 155
- Matsubayashi, T., Makino, J., & Ebisuzaki, T. 2007, *ApJ*, 656, 879
- Merritt, D., Gualandris, A., & Mikkola, S. 2009, *ApJ*, 693, L35
- Miller, M. C., & Colbert, E. J. M. 2004, *International Journal of Modern Physics D*, 13, 1
- Miralda-Escudé, J., & Gould, A. 2000, *ApJ*, 545, 847
- Morris, M. 1993, *ApJ*, 408, 496
- O'Leary, R. M., Kocsis, B., & Loeb, A. 2009, *MNRAS*, 395, 2127
- O'Leary, R. M., Rasio, F. A., Fregeau, J. M., Ivanova, N., & O'Shaughnessy, R. 2006, *ApJ*, 637, 937
- Peters, P. C. 1964, *Physical Review*, 136, 1224
- Peters, P. C., & Mathews, J. 1963, *Physical Review*, 131, 435
- Pfahl, E., & Loeb, A. 2004, *ApJ*, 615, 253
- Phinney, E. S. 2001, ArXiv eprints, astro-ph/0108028
- Portegies Zwart, S. F., Baumgardt, H., McMillan, S. L. W., Makino, J., Hut, P., & Ebisuzaki, T. 2006, *ApJ*, 641, 319
- Portegies Zwart, S. F., & McMillan, S. L. W. 2002, *ApJ*, 576, 899
- Preto, M., Berentzen, I., Berczik, P., & Spurzem, R. 2011, *ApJ*, 732, L26
- Rajagopal, M., & Romani, R. W. 1995, *ApJ*, 446, 543
- Ray, A., & Kluzniak, W. 1994, in *IAU Symposium*, Vol. 165, GA XXII, VT.145, ed. H. van Woerden
- Reid, M. J., & Brunthaler, A. 2004, *ApJ*, 616, 872
- Sesana, A. 2010, *ApJ*, 719, 851
- Sesana, A., Haardt, F., Madau, P., & Volonteri, M. 2004, *ApJ*, 611, 623
- Sesana, A., Vecchio, A., & Colacino, C. N. 2008, *MNRAS*, 390, 192
- Sesana, A., Vecchio, A., & Volonteri, M. 2009, *MNRAS*, 394, 2255
- Smits, R., Kramer, M., Stappers, B., Lorimer, D. R., Cordes, J., & Faulkner, A. 2009, *A&A*, 493, 1161
- Smits, R., Tingay, S. J., Wex, N., Kramer, M., & Stappers, B. 2011, *A&A*, 528, A108+
- van Haasteren, R., et al. 2011, *MNRAS*, 414, 3117
- Wex, N., Gil, J., & Sendyk, M. 1996, *A&A*, 311, 746
- Wyithe, J. S. B., & Loeb, A. 2003, *ApJ*, 590, 691
- Yu, Q., & Tremaine, S. 2003, *ApJ*, 599, 1129